COBEM 2021 26th International Congress of Mechanical Engineering
November 22-26, 2021, Virtual Congress, Brazil

COB-2021-0069
OPTIMIZATION OF BANDGAP FORMATION IN PERIODIC ROTORS

P. B. Lamas
R. Nicoletti
University of São Paulo, São Carlos School of Engineering, São Carlos-SP, 13566-590, Brazil
patrick.b.lamas@usp.br, rnicolet@sc.usp.br

Abstract. *Rotating machines with components periodically mounted along the shaft present band gaps in their frequency spectrum. That means, the natural frequencies of the rotor tend to group together, leaving some modal spacing in regions of the frequency spectrum. Such modal spacing is characterized by a large bandwidth where the structure presents no natural frequencies and a low frequency response. The bandwidth and the region where these band gaps appear depend on the geometry and on the inertia distribution of the periodic rotor. In the present work, we show that periodic rotors with two types of cells have bandgaps in their frequency spectrum. Also, we shown that is possible to shift the band gap towards higher or lower frequency regions of the spectrum of a given periodic rotor by optimizing the position of the rotor elements. The rotor is modeled by finite element method and the position of the impellers on the rotor is optimized by a direct search method (Sequential Quadratic Programming - SQP). The results show that it is possible to move the band gap without significantly affecting its bandwidth. The optimization of the band gap region represents an interesting tool in the design of rotating machines.*

Keywords: *metamaterial, periodic rotors, rotor dynamics, mechanical vibrations, finite element method.*

1. INTRODUCTION

Rotating machines, like turbines and gas compressors are mainly composed by a rotating shaft with working elements (impellers, blade stages, disks) mounted on it. These working elements adds localized mass and inertia in the system and, when these localized inertia are evenly distributed along the shaft, a dynamic effect occurs: zones in the frequency spectrum present high attenuation, thus forming a bandgap region in the frequency response function (FRF) of the system (Richards and Pines, 2003). These bandgap regions are characterized by the lack of resonances, low system's response to excitation, and bandwidth much bigger than the average distance between two resonances of the system (Deymier, 2013). These characteristics are interesting for rotating systems because they operate at specific frequency ranges. By placing a bandgap in the operating range of the machine will guarantee its low vibration response with a good safety margin.

Any periodic structure can present bandgaps in their frequency spectrum (Bachour and Nicoletti, 2020). In this case, periodicity has the effect of filtering the propagating waves in the structure, like phononic crystals and metamaterials (Deymier, 2013). Conceptually, periodic structures are structures composed of a number of identical structural elements, also called cells, linked together to form the complete structure in 1, 2 or 3 dimensions (Mead, 1996).

In rotors, the appearance of bandgaps can be achieved by geometric periodicity. Hence, by designing the rotor with a certain geometry, we can make the system present a bandgap region that can be used to attenuate the vibration response of the machine. Therefore, in this bandgap region, the system will be insensitive to any source of perturbation. In the literature, we can find rotors with periodic variation of the shaft diameter, with interesting results regarding the attenuation of torsional (Richards and Pines, 2003) and lateral vibrations Alsaffar *et al.* (2018). Also, there has been an effort to design periodic vibration absorbers for rotating systems (Yu *et al.*, 2006; Song *et al.*, 2013; Fan *et al.*, 2020). However, the effects of mounting the disks periodically along the rotor has not been studied yet, to the knowledge of the authors.

In the present work, we analyze whether it is possible to design rotors with bandgaps at desired frequency regions, and if it is possible to move these bandgaps regions towards higher or lower frequencies. To do that, we use two types of cells that compose the rotating periodic structure: a section of shaft with a single rigid disk (Fig. 1a), and a section of shaft with two different rigid disks equally displaced along the shaft section (Fig. 1b). We analyze the effect of the number of cells in the frequency spectrum of the system and we adopt an optimization procedure to allocate the bandgap in the frequency spectrum by changing the position of the disks mounted on the rotor (design variables of the optimization). The main contribution of this work is the methodology of designing the rotor with optimized periodic geometry to allocate the resultant bandgaps of the system at desired frequency regions.

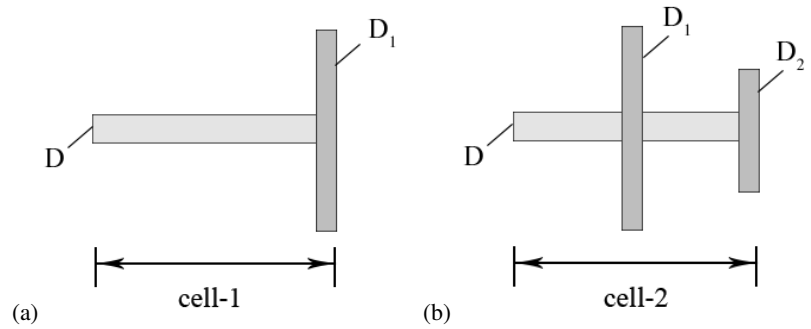

Figure 1. Cell types for the periodic rotors in study: (a) single-disk cell, (b) double-disk cell with different diameters.

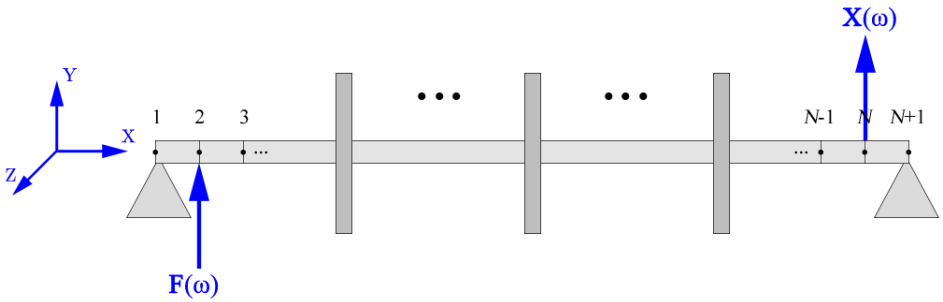

Figure 2. Finite element representation of the rotor with the excitation ($\mathbf{F}(\omega)$) and response ($\mathbf{X}(\omega)$) points used to calculate the FRF.

2. MATHEMATICAL MODELING OF THE ROTATING SYSTEM

Consider a periodic rotor with its working elements (impellers) evenly distributed along the shaft. The periodic structure can be formed by a cell-1 type or cell-2 type (Fig. 1). To study the bandgap formation in this rotor, we model the rotor by Finite Elements based on the rotor finite elements derived by Nelson and McVaugh (1976): the shaft is modelled by Euler-Bernoulli beam theory and the impellers are modelled by the rigid body dynamics (rigid disks with inertia properties). The shaft elements have constant area and material properties, and they have two nodes, each one with four degrees-of-freedom: translation in lateral directions (y_i and z_i), and rotation around $\mathbf{Y}$ e $\mathbf{Z}$ directions (β_i and γ_i) – Fig. 2. Considering a mesh with N connected elements to represent the shaft, one obtains the following system of ordinary differential equations:

$$\mathbf{M}\ddot{\mathbf{x}} - \Omega\mathbf{G}\dot{\mathbf{x}} + \mathbf{K}\mathbf{x} = \mathbf{F} \tag{1}$$

where $\mathbf{M}$, $\mathbf{G}$, and $\mathbf{K}$ are the inertia, gyroscopic, and stiffness matrices, respectively, Ω is the rotating speed (in rad/s), $\mathbf{x}$ is the vector of nodal displacements composed by all degrees-of-freedom of the shaft, $\dot{\mathbf{x}}$ is the vector of nodal velocities, $\ddot{\mathbf{x}}$ is the vector of nodal accelerations, and $\mathbf{F}$ is the vector of external forces applied to the nodes of the model.

Hence, the vector of all degrees-of-freedom of the shaft, composed by the linear and angular displacements of the nodes of the model, is given by:

$$\mathbf{x} = \{y_1\ z_1\ \beta_1\ \gamma_1\ \cdots\ y_i\ z_i\ \beta_i\ \gamma_i\ \cdots\ y_{N+1}\ z_{N+1}\ \beta_{N+1}\ \gamma_{N+1}\}^T \tag{2}$$

The inertia of the rigid disks that represent the rotor impellers are coupled to the model depending on the node the disk (impeller) is attached to. The detailed formulation of the finite elements as well as the finite element matrices are presented in Nelson and McVaugh (1976).

By adopting this model, the natural frequencies of the rotor are calculated by solving the eigenvalue problem of the system, given by:

$$(-\omega^2\mathbf{M} - i\omega\Omega\mathbf{G} + \mathbf{K})\mathbf{u} = 0 \tag{3}$$

The frequency response function of the system is analyzed calculating the receptance matrix, given by:

$$\mathbf{H}(\omega) = \frac{\mathbf{X}(\omega)}{\mathbf{F}(\omega)} = (-\omega^2\mathbf{M} - i\omega\Omega\mathbf{G} + \mathbf{K})^{-1} \tag{4}$$

In this work, all the results are based on the response in vertical direction of the first unconstrained node next to the first bearing due to an excitation in vertical direction at the last unconstrained node next to the second bearing (opposite side of the shaft) – see Fig. 2. In all analyses, the bearing allows rotational motion only (lateral displacements are constrained), thus representing the configuration of simply-supported rotor. As a rule, we adopt 10 finite elements between two disks or between a disk and a bearing (a number of elements large enough to assure natural frequency convergence).

3. BANDGAP FORMATION IN PERIODIC ROTORS

The properties of the rotors in study are presented in Table 1. Figure 3 presents the numerical results of natural frequencies and FRF amplitude for the two types of rotor in study. The results are presented as a function of the number of cells that compose the rotor, and they refer to the case of null rotating speed for sake of clarity (the effect of the rotating speed on the results will be presented at the end of this section). As we can see in Fig. 3, by increasing the number of cells, two bandgaps are created for the cell-1 type rotor, whereas four bandgaps are created for the cell-2 type rotor (indicated by numbers).

Table 1. Properties of the rotors in study.

Property	**Value**	**Unit**
shaft length (L)	600	mm
shaft diameter (D)	5	mm
disk diameter (D_1 and D_2)	40 / 30	mm
disk thickness (E_d)	5	mm
Young modulus (E)	2.1×10^{11}	$\mathrm{N.m^{-2}}$
material density (ρ)	7850	$\mathrm{kg.m^{-3}}$

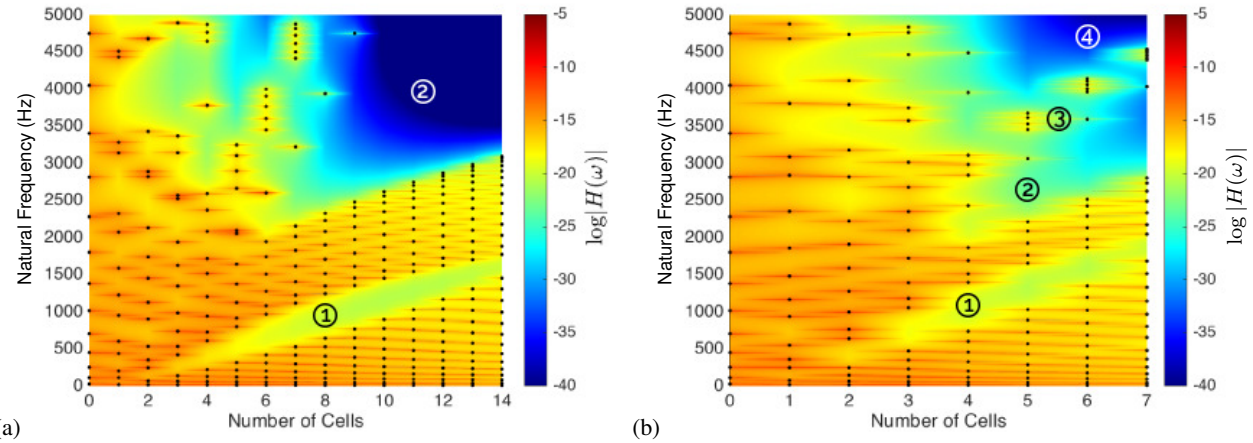

(a) (b)

Figure 3. Natural frequencies (dots) and the amplitude of the FRF (colors) of the rotors as a function of the number of disks evenly distributed along the shaft (results for null rotating speed): (a) cell-1 type rotor, (b) cell-2 type rotor.

The first bandgap has the maximum bandwidth of 600 Hz for the cell-1 rotor with 8 cells (8 disks), and 659 Hz for the cell-2 rotor with 4 cells (8 disks). This bandgap is created after the N_D-th natural frequency of the rotors, being N_D the number of disks in the system. Therefore, the start frequency of bandgap #1 is the N_D-th natural frequency and the stop frequency of this bandgap is the $(N_D + 1)$-th natural frequency. This bandgap is formed by the matching between the position of the disks and the eigenmode wavenumber, as illustrated in Figs. 4 and 5. Such effect is observed in rotors with any number of disks.

In the case of bandgap #2, the gap appears after the $2N_D$-th natural frequency for the cell-1 type rotor and after the $3N_D/2$-th natural frequency for the cell-2 type rotor. In this case, the bandgap does not appear due to the matching of the eigenmode wavenumber and the position of the disks. This second gap is formed by the presence of localized mode shapes, where the disks barely move and vibration occurs in localized sections of the shaft, as illustrated in Figs. 6 and 7. In this case, the bandwidth of the gap much bigger than that of bandgap #1, and this effect is observed in rotors with any number of cells.

Bandgap #3 is only present in the cell-2 type rotor. This gap appears between the $(3N_D/2 + 1)$-th natural frequency and the $(3N_D/2 + 2)$-th natural frequency. Note that, the start frequency of this gap is also the stop frequency of bandgap #2. Bandgap #3 is created by the impedance matching. However, this match occurs only at the disks with diameter D_2.

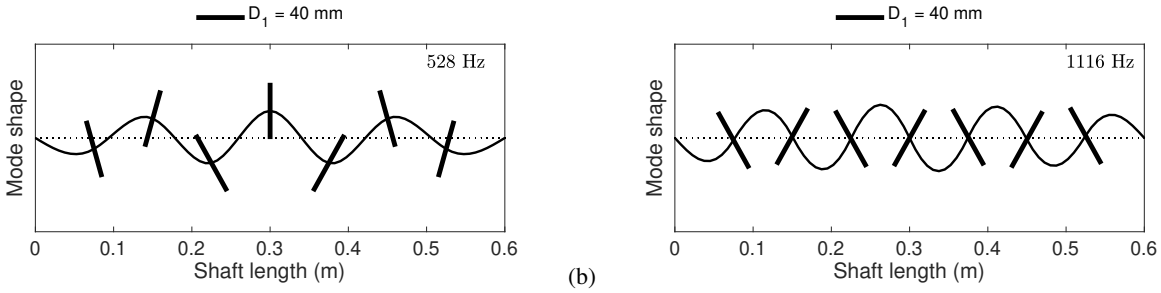

Figure 4. Mode shapes of the cell-1 type rotor with 7 cells (7 disks): (a) 7th mode shape (start of bandgap #1), (b) 8th mode shape (stop of bandgap #1).

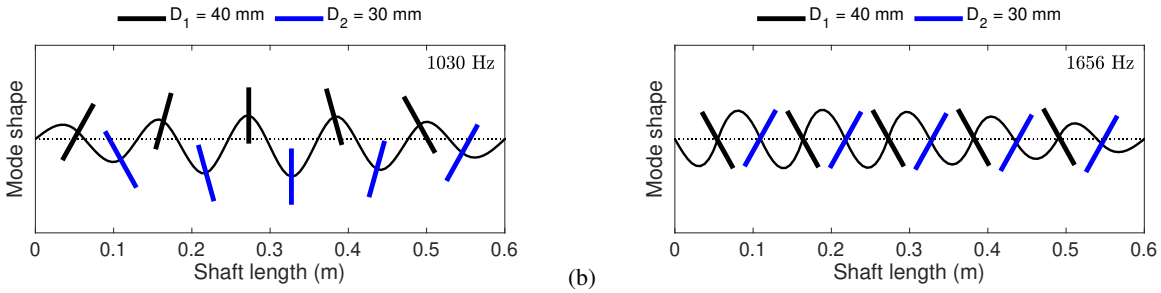

Figure 5. Mode shapes of the cell-2 type rotor with 5 cells (10 disks): (a) 10th mode shape (start of bandgap #1), (b) 11th mode shape (stop of bandgap #1).

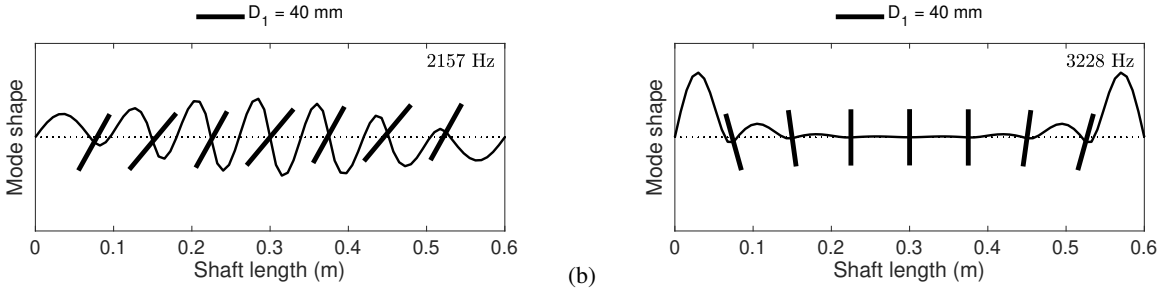

Figure 6. Mode shapes of the cell-1 type rotor with 7 cells (7 disks): (a) 14th mode shape (start of bandgap #2), (b) 15th mode shape (stop of bandgap #2).

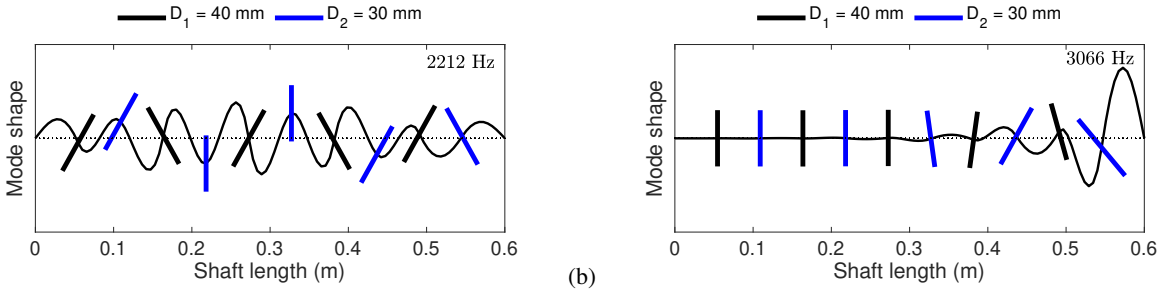

Figure 7. Mode shapes of the cell-2 type rotor with 5 cells (10 disks): (a) 15th mode shape (start of bandgap #2), (b) 16th mode shape (stop of bandgap #2 and start of bandgap #3).

We can see that by looking at mode shape of the bandgap #3 stop frequency (Fig. 8). Such effect is also observed in cell-2 type rotors with any number of disks.

In fact, it is expected that different elements in the cell result in a new gap in the frequency spectrum. Note that the cell-1 type rotor is a particular case of cell-2 type rotors, in which $D_1 = D_2$. Then, when $D_1 \neq D_2$ there appears this new bandgap in the frequency spectrum, and this new bandgap is related to this different disk in the cell (D_2). This was

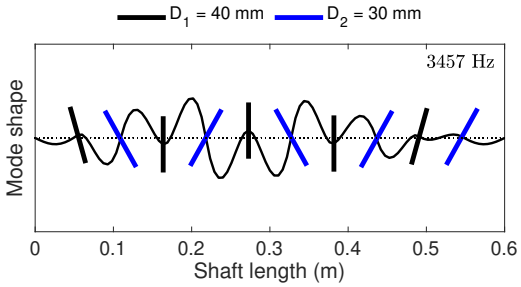

Figure 8. Mode shape of the cell-2 type rotor with 5 cells (10 disks): 17th mode shape (stop of bandgap #3).

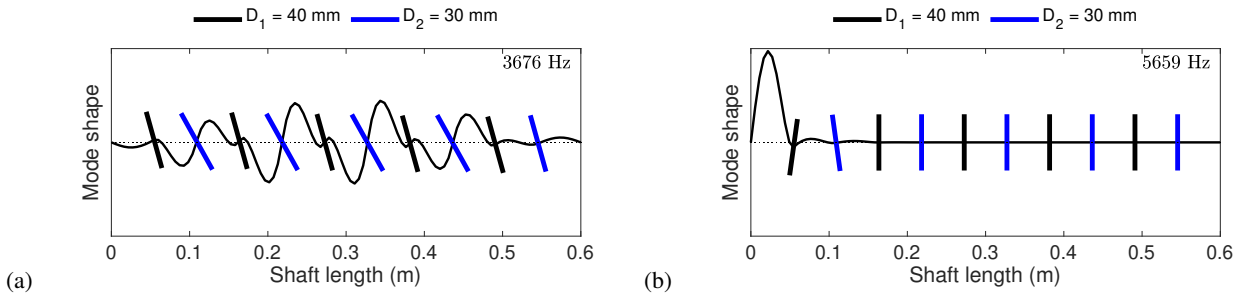

Figure 9. Mode shapes of the cell-2 type rotor with 5 cells (10 disks): (a) 20th mode shape (start of bandgap #4), (b) 21th mode shape (stop of bandgap #4).

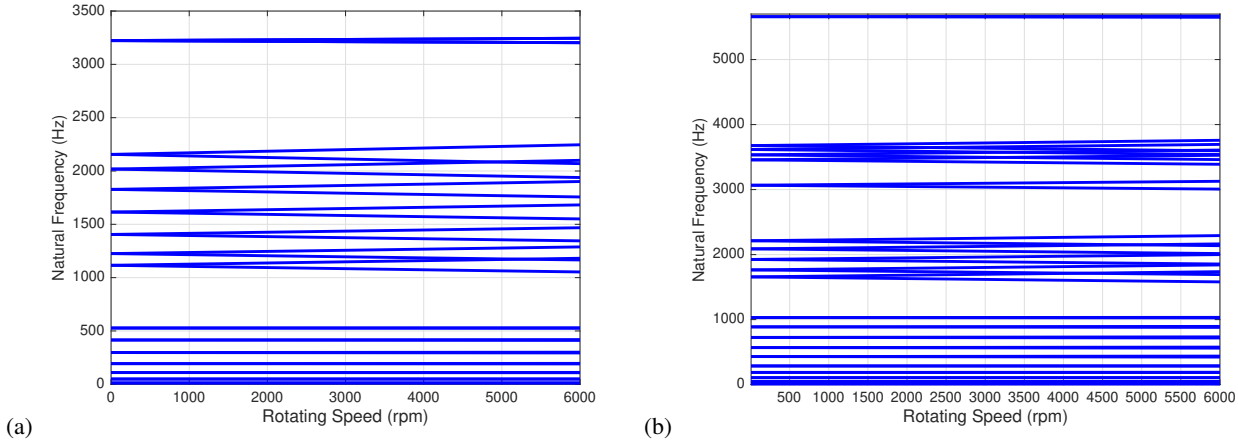

Figure 10. Campbell diagram of the studied rotors: (a) cell-1 type rotor with 7 cells (7 disks), (b) cell-2 type rotor with 5 cells (10 disks).

also observed by El-Borgi *et al.* (2020), where the authors shown that for beams with mass-spring resonators periodically distributed, using a cell like cell-2 type, i.e. a cell with two resonators tuned in different natural frequencies, two bandgaps in the beam frequency spectrum are created, while only one bandgap is created when the resonators are tuned at the same natural frequency.

In the case of bandgap #4, the gap appears between the $2N_D$-th and $(2N_D + 1)$-th natural frequencies and it is present only for the cell-2 type rotor. Bandgap #4 is created by the presence of localized mode shapes, where the disks barely move and vibration occurs in localized sections of the shaft, as illustrated in Fig. 9. This effect is also observed in rotors with any numbers of cells.

The results in Fig. 3 were obtained with null rotating speed. To investigate the influence of the rotating speed, a Campbell diagram is presented in Fig. 10 for both cell-1 and cell-2 type rotors. As one can see, the natural frequencies split into two frequencies, which are associated with two precession modes (forward and backward) caused by the gyroscopic effect. This effect is magnified with increasing rotating speeds. As a result of the gyroscopic effect, the bandgap tends to narrow as the rotating speed increases. In the cell-1 type rotor (Fig. 10a), the first bandgap narrows by 11% at the rotating speed of 6,000 rpm, whereas the second bandgap decreases by 10%. In the cell-2 type rotor (Fig. 10b), the first bandgap

narrows by 13% at the rotating speed of 6,000 rpm; the second bandgap decreases by 16%, the third bandgap narrows by 33%, and the fourth bandgap decreases by 4%. Although we have a narrowing in the bandgaps, the use of the bandgaps is not impaired. The bandgaps are still large enough for a safe machine operation.

In this section, we showed that periodic rotors with cell types like cell-1 and cell-2 do present bandgaps in their frequency spectrum. This occurs due to two different reasons: impedance matching and localized modes. The gyroscopic effect tends to narrow the bandwidth of the gaps, but the bandwidth of the bandgaps is still large enough for a safe machine operation. The question now is whether we can move these bandgaps towards desired frequency regions by making small changes in the position of the impellers leading to a quasi-periodic configuration. For that, we employ an optimization procedure.

4. BANDGAP POSITIONING IN PERIODIC (OR QUASI-PERIODIC) ROTORS

To analyze the positioning of the bandgaps we employ an optimization procedure. The optimization problem is categorized as a mono-objective, multi-variable, constrained, and non-linear optimization (Rao, 2009).

4.1 Optimization Procedure

The approach used to allocate the bandgaps is based on two considerations: 1) move the central frequency of the bandgap towards a desired value, and 2) maximize the bandwidth of the bandgap around the desired central frequency. This is made by only making changes in the position of the impellers. Thus, the design variables of the optimization procedure are:

$$\mathbf{q} = \{x_1 \cdots x_i \cdots x_{N_D}\}^T \tag{5}$$

where $\mathbf{q}$ is the design variables vector, x_i are the impellers coordinates along the shaft in the axial direction, and N_D is the number of impellers.

Hence, we state the optimization problem as:

$$\arg\max \ f(\mathbf{q}) = \Delta\omega(\mathbf{q}) \tag{6}$$

subject to:

$$g_1(\mathbf{q}) = |x_{i+1} - x_i| \geq 30\ mm \tag{7}$$

$$g_2(\mathbf{q}) = |\omega_{central} - \omega_{desired}| \leq 1\ Hz \tag{8}$$

where the constraint $g_1(\mathbf{q})$ limits the optimized distance between the impellers to be greater than 30 mm. The distance between the impellers next to bearings was constrained to be greater than 30 mm. The constraint $g_2(\mathbf{q})$ establishes a acceptable tolerance between the desired central frequency ($\omega_{desired}$) and the central frequency obtained by the optimization procedure ($\omega_{central}$). The objective function in Eq. (6) will maximize the bandwidth of the bandgap ($\Delta\omega$) around the desired central frequency of the bandgap.

A direct search method (Rao, 2009) is employed to find the optimum solutions. Because direct methods need an initial point to start the search, we used the periodic configuration as the starting point for shifting the central frequency of the bandgap by ± 1 %. To shift the bandgap by ± 2 %, we use as initial point the solution that shift the bandgap by ± 1 %, and so on. The adopted algorithm was the Sequential Quadratic Programming (SQP). We ran the SQP with a maximum of 50 iterations with a function convergence toleration of 10^{-16}. The whole algorithm was programmed in MATLAB.

4.2 Numerical Results

Considering the cell-1 and cell-2 type rotors, and adopting the optimization procedure described above, one arrives to the results presented in Fig. 11 for the positioning of the bandgap 1 in both rotors. Figure 11 displays the FRF of the optimized rotors when the central frequency is moved towards the maximum possible allocation to higher and lower central frequencies than the central frequency of the bandgap in the periodic rotor. The hot colors represent high amplitude response, while the cold ones represent low amplitude responses. The bandgap region is the blue zone around the $\omega_{central}$ line. As one can see from Fig. 11, the optimization procedure successfully found configurations that shifted the bandgap according to the desired value.

Figure 12 displays the optimized positions of the impellers (black dots) for the cell-1 and the cell-2 type rotors. Note that in Fig. 12b, for the case of $\Delta\omega_{central} = 0$, the position of the impellers do not match the periodic positions (blue dashed lines). That is a consequence of the optimization procedure, which maximizes the bandgap even for the original case ($\Delta\omega_{central} = 0$).

The optimization procedure presented a limitation in the maximum variation of the bandgap central frequency. The upper and lower limits are different for both rotor types in study. How much it is possible to move the bandgap strongly

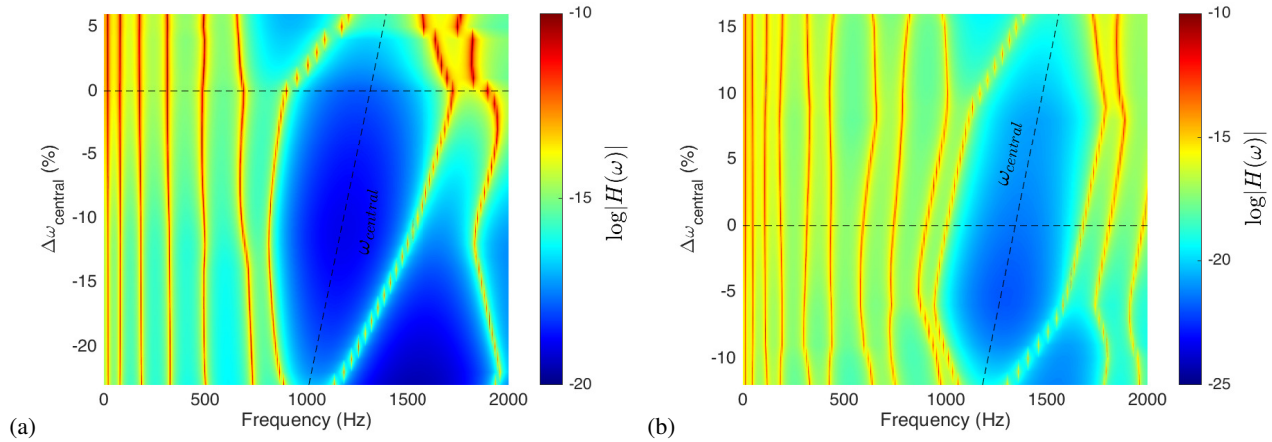

Figure 11. Frequency response function of the optimized rotors as a function of the variation of the central frequency $\Delta\omega_{central}$ (results for null rotation): (a) cell-1 type rotor with 7 cells (7 disks), (b) cell-2 type rotor with 5 cells (10 disks).

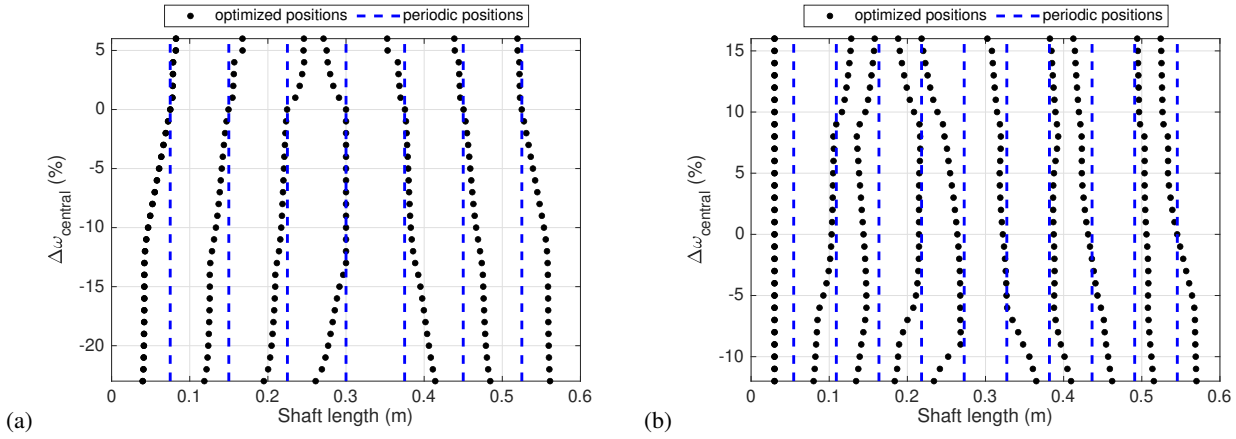

Figure 12. Optimized positions of the impellers on the shaft as a function of the variation of the central frequency: (a) cell-1 type rotor with 7 cells (7 disks), (b) cell-2 type rotor with 5 cells (10 disks).

depends on the number of impellers, on the inertia of the impellers, on the inertia of the shaft, and on the stiffness of the shaft. Also, it is worth emphasizing that the optimized rotors are no longer periodic, they are quasi-periodic rotors.

5. CONCLUSION

This work presents a methodology to design rotating machines with minimum response in a given frequency range with a good safety margin. The obtained results led to the following conclusions:

- periodic rotors with cell-1 or cell-2 type structures present bandgaps in their frequency spectrum;
- bandgaps in periodic rotors occurs due to impedance matching and localized mode shapes;
- the allocation of bandgaps towards higher or lower frequencies can be done by changing the inertia distribution of the impellers on the shaft;
- the positioning of the bandgaps is limited and it is strongly affected by the inertia of the impellers, the inertia of the shaft, the number of impellers, and the stiffness of the shaft;
- the rotors with optimized positions are quasi-periodic.

6. ACKNOWLEDGEMENTS

This project was supported by the Brazilian research foundations FAPESP (Fundação de Amparo à Pesquisa do Estado de São Paulo), under grant no. 2018/15894-0 (ENVIBRO Project), CNPq (Conselho Nacional de Desenvolvimento Científico e Tecnológico), under grant no. 301118/2018-3, and CAPES (Coordenação para o Aperfeiçoamento de Pessoal de Nível Superior), under grant no. 88887.484667/2020-00.

7. REFERENCES

Alsaffar, Y., Sassi, S. and Baz, A., 2018. "Band gap characteristics of periodic gyroscopic systems". *Journal of Sound and Vibration*, Vol. 435, pp. 301–322. doi:10.1016/j.jsv.2018.07.015.

Bachour, R.S. and Nicoletti, R., 2020. "Natural frequencies and band gaps of periodically corrugated beams". *Journal of Vibration and Acoustics*, Vol. 143, No. 4. doi:10.1115/1.4048889.

Deymier, P.A., ed., 2013. *Acoustic Metamaterials and Phononic Crystals*. Springer Berlin Heidelberg. doi:10.1007/978-3-642-31232-8.

El-Borgi, S., Fernandes, R., Rajendran, P., Yazbeck, R., Boyd, J. and Lagoudas, D., 2020. "Multiple bandgap formation in a locally resonant linear metamaterial beam: Theory and experiments". *Journal of Sound and Vibration*, Vol. 488, p. 115647. ISSN 0022-460X. doi:https://doi.org/10.1016/j.jsv.2020.115647.

Fan, L., He, Y., Chen, X. and Zhao, X., 2020. "Elastic metamaterial shaft with a stack-like resonator for low-frequency vibration isolation". *Journal of Physics D: Applied Physics*, Vol. 53, p. 105101.

Mead, D., 1996. "Wave propagation in continuous periodic structures: Research contributions from southampton, 1964–1995". *Journal of Sound and Vibration*, Vol. 190, No. 3, pp. 495–524. ISSN 0022-460X. doi: https://doi.org/10.1006/jsvi.1996.0076.

Nelson, H.D. and McVaugh, J.M., 1976. "The Dynamics of Rotor-Bearing Systems Using Finite Elements". *Journal of Engineering for Industry*, Vol. 98, No. 2, pp. 593–600. ISSN 0022-0817. doi:10.1115/1.3438942.

Rao, S., 2009. *Engineering Optimization: Theory and Practice*. Wiley. ISBN 9780470183526.

Richards, D. and Pines, D., 2003. "Passive reduction of gear mesh vibration using a periodic drive shaft". *Journal of Sound and Vibration*, Vol. 264, No. 2, pp. 317–342. doi:10.1016/s0022-460x(02)01213-0.

Song, Y., Wen, J., Yu, D. and Wen, X., 2013. "Analysis and enhancement of torsional vibration stopbands in a periodic shaft system". *Journal of Physics D: Applied Physics*, Vol. 46, p. 145306.

Yu, D., Liu, Y., Wang, G., Cai, L. and Qiu, J., 2006. "Low frequency torsional vibration gaps in the shaft with locally resonant structures". *Physics Letters A*, Vol. 348, No. 3-6, pp. 410–415. doi:10.1016/j.physleta.2005.08.067.

8. RESPONSIBILITY NOTICE

The authors are solely responsible for the printed material included in this paper.